SLAC-PUB-5002
June 1989
(I)

A REVIEW OF 4π ČERENKOV RING IMAGING DETECTORS[‡]

DAVID W. G. S. LEITH

Stanford Linear Accelerator Center
Stanford University, Stanford, California 94309

ABSTRACT

The design choices for 4π ring imaging Čerenkov counters-both those of principle and those of practice-are reviewed. The progress in construction and the performance of the devices being built for DELPHI and SLD are discussed.

Invited talk presented at the Symposium on
Particle *Identification at High Luminosity Hadron Colliders*
Batavia, IL, April 5–7, 1989.

[‡] Work supported by Department of Energy contract DE–AC03–76SF00515.

Introduction

This talk is *not* about particle identification in experiments at high-luminosity hadron colliders, as the title of this symposium suggests. Instead, the purpose of this talk is to review the status of the two full-coverage, ring imaging detectors currently being built-the RICH system[1] in the DELPHI experiment at LEP and the CRID system[2] in the SLD experiment at SLAC. We will recount the experiences and the design choices made in these two experiments, and summarize how well the devices being built actually do perform.

Figure 1 shows the layout of the SLD experiment. It is representative of all the high energy e^+e^- experiments in that it consists of nested subsystems, each of which contributes independent information on the events under study. Figure 1 is a schematic quadrant view showing each of the subsystems and indicating the projective tower structure of the calorimeter, both in the Liquid Argon and in the Warm Iron segments.

The principle of both the DELPHI and SLD ring imaging detectors is summarized in Figs. 2(a) and 2(b). There are two radiators-l cm of a liquid and 45 cms of a gas-to give maximum coverage of the momentum range under study in Z^0 decay. Light from the thin liquid radiator falls on the front face of a long drift detector box, while light-from the gas radiator is optically focused onto the back face of the same particle detector box. The image of the liquid radiator light (for normally incident particles) forms a 17 cm radius circle of $\approx$ 1.5 cm width, and has about 25 photoelectrons distributed around the circumference. The gas radiator light is focused to a 3 cm radius ring of about 2 mm thickness and with about 12 photoelectrons. The Cerenkov light is detected in the long drift boxes via photoionization of a minority component ($\approx$ 0.1%) of the drift gas, called TMAE, or tetrakis-(Dimethylamino)-ethylene. The photoelectron drifts under the influence of a uniform electric field, to a multiwire proportional chamber. The coordinates of the point of origin of the photoelectron are measured from the drift time, the wire address, and by the charge division on each end of the MWPC anode wire to determine the position of the avalanche along the length of the wire. These three coordinates are measured with an accuracy of $\approx \pm 1$ mm, resulting in a determination of the Cerenkov angle to $\approx$ 1%. This allows particle identification e/π, π/K, and K/π as shown in Fig. 3. The potential utility of such hadron identification is shown in Fig. 4, where heavy quark tagging in Z^0 decays is demonstrated, applying first the vertex detector information, then the particle identification, and finally both together.[3] Clean and efficient heavy quark tagging can be clearly achieved with the help of the ring imaging detectors. Finally, Fig. 5 shows experimental data on the π, K separation achieved using the SLD prototype Cerenkov counter in an 11 GeV/c test beam at SLAC.[4] Impressive π, K separation is observed.

An example of the mechanical realization of these detectors is sketched in Fig. 6. There are three separate vessels-the Barrel unit, and two End Caps— which close the solid angle coverage. For the Barrel, the components (the mirror ladders, the drift box and detectors, and the liquid radiator trays) are inserted through 10 sector openings at each end. A G-10 central plane serves as both the center mechanical support for each of the components and as a distributor of 60 kV high voltage to each of the drift boxes.

So much for a brief overview of the 4π ring imaging counters. Let us now consider first the problem of principle and then the problems of practice that one faces when designing such a device. We will then review how well these new devices are really performing.

Problems of Principle

When designing a Cerenkov Ring Imaging Detector, one has to face several basic design choices. I list the individual items, and then go on to discuss them topic by topic:

- Radiator
- Photocathode
- Optics scheme
- Electron detector design and third coordinate readout
- Photon feedback protection.

Radiator

The choice of radiator is driven by the requirement that it be transparent to light of the wavelength of interest and that the index of refraction be appropriate for the momentum range under study. The threshold velocity for Cerenkov radiation is given as $\gamma_{th} = 1/\sqrt{1-(1/n^2)}$, where n is the index of refraction. Table I, shows the radiators chosen by four experiments employing ring imaging technology, including the two experiments under review in this paper. The performance, in terms of particle identification, of the two radiators has already been spelled out in Fig. 3. The variation of Cerenkov angle for each radiator, for e, π, K, and p is shown in Fig. 7, as a function of particle momentum. One can quickly see that if an angular resolution of l-2 mrad can be achieved, excellent particle identification may be achieved over a broad momentum region.

Photocathode

In recent years, only two photocathodes have been widely used, although there is an interesting effort in “designer-molecular chemistry” underway to develop alternative materials.[5] The photocathode is a carrier gas with a minority mixture of a photoionizing agent-either triethylamine (TEA) or tetrakis dimethylamine ethylene (TMAE). The properties of these photocathode materials are summarized in Table II.

For large-area systems, TEA is not favored, as it requires expensive CaF windows and requires very clean gas in the radiator volume to avoid the loss of Cerenkov photons at the wavelength one wishes to detect. TMAE is more forgiving, both in the cost of window material and in the required cleanliness (or removal of oxygen and water vapor) of the gas radiator system. The disadvantages of TMAE are its low vapor pressure (which results in a long Cerenkov photon absorption length) and the high electronegativity of the chemical reaction products.[6]

Optics

The choice of the optics for a ring imaging system, as described in Fig. 2(a) above, is driven by the requirement to keep the contribution to the measurement error due to the focusing system small when compared to other errors. The various sources of error are well described in Tom Ypsilantis' 1980 talk on Cerenkov Ring Imaging for LEP experiments[7] and in Tord Ekelof's 1984 SLAC Summer School lectures.[8]

The two experiments choose different solutions to this problem. DELPHI uses larger area mirrors and has developed a new fabrication technique which uses no grinding and polishing, and preserves the virgin surface of the float glass blanks used to form the mirrors. To keep the errors due to optical distortion acceptable, they slump parabolic mirrors. They have successfully produced all of their mirrors, with the help of Bofors Co., and have achieved excellent UV reflectivity and surface flatness.' The average reflectance of all the DELPHI mirrors is greater than 85% for the wavelength range (1650—2000)Å.

For SLD, the optics design employs two ladders of five (27 x 30) cm mirrors, reflecting the light back to each drift box. With this size mirror, SLD can comfortably use spherical mirrors. The mirrors for the Barrel counter have all been produced by Lancaster Corp. and coated by Acton Co. They are 6 mm thick float glass pieces which are rapidly slumped in a mold in a gas oven, annealed and then ground and polished to the required surface finish. The blanks are then checked for dimensions, radius of curvature, local flatness and optical distortion; those passing, were sent to Acton Co. for a good UV reflectance coating. Figure S(a) is the data from a detailed surface profile measurement of these mirrors, showing 26 Å rms features on the mirror surface; Fig. 8(b) displays the reflectance as a function of wavelength for the first 100 mirrors produced.

Electron Detector

The choice of design for the electron detector for a Cerenkov Ring Imaging counter has to accommodate several requirements. The detector scheme is schematically shown in Fig. 9, where the Cerenkov photon is seen entering the photocathode region and photoionizing the TMAE gas. The long absorption length in TMAE results in a parallax error which must be removed by measuring the depth at which the electron was produced (i.e., the third coordinate). So the drift time and wire address come fairly straightforwardly, but the technique used to measure this third coordinate is something of a challenge.

-Figure 10 shows the electron detection mechanism-the formation of a Townsend avalanche near the surface of the anode wire of the MWPC. The formation of the avalanche leaves the gas in an excited state, and a substantial fraction of this time the return to the ground state is achieved by photon emission. The very high efficiency TMAE photocathode provides the engine for a strong positive feedback situation which must be controlled in an effective detector design.

The solution chosen by the DELPHI experiment is shown in Fig. 11. The anodes are 20 μm tungsten wires strung on a pitch of 2.6 mm. The third coordinate is read out by cathode strips, as shown in the figure. To achieve good efficiency for the cathode readout, close coupling of the anode is necessary, resulting in 0.5 mm -anode-to-cathode spacing. The cathode strips are 5.4 mm wide and 42 mm long, covering 16 anode wires. The large signal developed by the energy loss from the passage of a charged particle represents a challenge for this method in that the large signal is capacitatively coupled to neighboring anodes unless clever precautions are taken. A resolution of 2 mm in this coordinate measurement has been achieved by the DELPHI group.[10] The protection against photon feedback is achieved by the blinds erected between wires, as displayed in Fig. 11. They are 1 cm high alumina blinds with field defining wires placed along the wall to shape the electric field guiding the electrons onto the MWPC anode. This structure interdicts wire-to-wire paths, and limits the opening angle back into the drift volume to $\approx 14^\circ$.

The SLD solution is shown in Fig. 12. The third coordinate is interpreted by a charge division measurement on the MWPC anodes. To achieve the required resolution, very resistive wires must be used. The SLD chamber is strung with 7 μm diameter carbon monofilaments, with a linear resistance of about 40 $K\Omega$ for the 10 cm length. The anodes are strung on a 3.2 mm pitch. A resolution of ± 0.7 mm is achieved in reading out the position of the avalanche along the length of the wire.[11] The photon feedback is tamed by machining U-shaped troughs in the cathode, giving wire-to-wire shielding. The backstreaming opening angle is limited to $\approx 5^\circ$ by a series of copper sheets, each at graded potential to properly control the electric drift field, and etched with 1 mm slots of metal removed in front of each anode. The observed photon feedback is shown in Fig. 13 as a function of the chamber voltage or, equivalently, of the gas gain.[12] A feedback level of $\approx 1\%$ is observed for normal operating conditions of the CRID.

Results of the charge division are shown in Fig. 14, from an average gas gain of 2×10^5. The resolution in determining the position of this avalanche along the 7 μm carbon wire is shown in Fig. 15 and indicates a measurement of $\sim 0.8\%$ of the wire length, or $\sim \pm 0.7$ mm.

Both detector solutions-that from DELPHI and from SLD-have been shown to perform satisfactorily and with the required accuracy to result in excellent particle identification over the momentum range to be examined in Z^0 decays.

Table III summarizes the various choices of principle made by these two experiments.

Problems of Practice

Moving from issues of principle to choices of practice, I list a number of areas of concern that require attention when designing and commissioning a ring imaging detector. They are:

- choice of the drift gas-for long drift box
- cleanliness of the gases ★
- choice of construction materials
- operating temperature
- implementation of the electrostatics *
- choice of the H.V. operating point ★
- gating *
- wire aging in TMAE environment ★
- calibration/monitoring of drift box/detectors. *

I will not have time to discuss all of these points, but will make some comments on each of the starred items.

Gas Cleanliness

The radiators have to be kept clean, with low contamination of oxygen and water vapor, to reduce the absorptive losses of UV photons. The drift gas also has to be kept free of oxygen and water vapor in order to minimize the electron capture losses of the precious photoelectrons as they drift of the order of 1 m in the long drift boxes (see Sec. I). In addition, we found that the commercially available TMAE comes with substantial contamination of highly electronegative components. In Fig. 16, we show gas chromatograph plots of regular, commercial TMAE and carefully washed TMAE, indicating the removal of much of the contamination.[6]

Electrostatics

The photocathodes in both of these experiments are TMAE-gas filled, quartz windowed boxes, with uniform electric fields along the box axis, guiding the drifting photoelectrons towards the MWPC detector. The method of producing the electric field in the two experiments is rather different.

For DELPHI, the boxes are made from quartz on all four sides, glued together to form a gas-tight structure. The field cage is made with metal strips evaporated onto the quartz. This has the very real advantage of having the dialectric surface in intimate contact with the conductors defining the drift field. It has the nuisance that it is difficult to make the electrical connections to the evaporated stripes.

For SLD, the boxes are made with G-10 printed circuit board sides and quartz windows, top and bottom. A photograph of the inner core of an SLD drift box during assembly is shown in Fig. 17. The sides in these boxes are double-walled, with a purge gas flowing in the side volume to reduce the risk of the very electronegative freon gas radiator leaking into the drift volume. The field cage is formed using etched arrays stretched on tooling fixtures and glued to both sides (inner and outer) of each quartz window of the box. The etched arrays are fabricated by etching away most of the metal from a 100 μm sheet, 150 x 50 cm of BeCu. What remains are 70 μm wires every 3 mm, with solder tabs at each end and a wide ribbon around the border for handling and for mounting on the tooling fixtures. This fabrication method creates highly reproducible wire frames which can be very precisely placed with respect to tooling heads in the border frames. Reproducibility from window to window and from inside to outside on a given window is $\pm 20\ \mu m$ over 130 cm. These are reasonably easily assembled on the windows; semiautomatic soldering techniques provide the electrical connection. The disadvantage in this construction is that the etched-array wire is not in intimate contact with the quartz and may allow polarization of the dielectric under certain conditions. So far in our prototype tests, we have not observed such effects.

Gating

The principle of Cerenkov photon detection was described in the Introduction and in Fig. 2. The uniform electric drift field, which guides the photoelectrons along the length of the long drift boxes and towards the multiwire proportional detector, is terminated on a grid of 100 μm tungsten wire strung on a pitch of 3.2 mm for the SLD device. The drifting electrons then experience a transfer field which sweeps it onwards into the etched array stack and focuses it down onto the anode wire, where it avalanches to a swarm of $\sim 10^5$ electrons. For the DELPHI detector, the drift field is similarly terminated.

The nominal electron drift path and the corresponding drift path of the returning positive ions are shown as the left-hand diagrams in Fig.. 18.

To protect the MWPC from premature aging and to avoid the buildup of charge on the walls of the long drift box, both the SLD and DELPHI experiments employ a gating circuit which switches +350 V and -350 V relative to the nominal voltage on alternate wires of this grid of 100 μm wires (see Fig. 18). When the gate is closed (i.e., when the f350 V is applied), no electrons drifting from the long drift box may enter the detector and no positive ions may escape from the detector; see the right-hand drawing in Fig. 18.

A typical operation in the SLD will be to open the gate with each e^+e^- crossing of the SLC (a 120 Hz operation) and close it again after about 40 μs. In this case, only electrons associated with events at the e^+e^- crossing will be detected, and the gate may be inhibited during poor operating conditions of the machine. The positive ions from the Townsend avalanche that caused the detection of a photoelectron will have only moved a few mm through the etched array stack before the gate closes, and so will never enter the drift box volume.

-Wire Aging

The addition of TMAE to regular drift chamber gas mixtures appears to drastically reduce chamber lifetimes.[13] We have measured such behavior for several different gas mixtures, flow rates, and for different size anode wires. When a chamber that shows such a loss in gain is opened and the anode surface exposed to air, droplets form on the anode; see Fig. 19. The deposit on the anode may be effectively cleaned by washing the chamber in ethanol. Normal operation is observed when the chamber is again put into service. For the SLD device, we have made serendipitous use of the resistive anodes! A d.c. current of ~ 10 m.a. applied for about 15 minutes raises the surface temperature of the anodes to > 400°C and “self cleans” the chamber by burning off the residue. In Fig. 20, a series of “deaths” of an SLD electron detector is shown, with subsequent “rebirth” after the required 15 minute “cooking.”

This should be an effective maintenance method for controlling the gain losses due to TMAE dissociation products depositing on the anodes.

Performance

Having discussed how these two experiments have been designed and put together, we should now ask how well they actually perform.

Figure 21 shows the angular resolution from both the liquid radiator and the gas radiator, as measured in the CERN tests of the DELPHI RICH prototype. Examples of single events showing π, K separation at 11 GeV/c and e, π separation at 4 GeV/c are shown in Fig. 22 for the SLD CRID prototype. The measured Cerenkov ring radius for 11 GeV/c, π's and K's for the SLD prototype was shown in Fig. 5 above. The pion ring radius is measured to an accuracy of f0.8 mm, corresponding to the result of measuring $\sim$ 12 photoelectrons on the Cerenkov circle, each one measured with an accuracy of $\sim$ 2.1 mm. Very clean π, K separation is observed.

-Table III summarizes the results for the prototype program of both SLD and DELPHI. Both experiments have achieved good N_0, observing $\sim$ 12 photoelectrons on the gas ring and $\sim$ 25 photoelectrons for the liquid radiator. The spatial accuracy for reconstructing the point of origin of the photoelectron allows measurement of the gas Cerenkov angle to $\pm$ (1–2)%, and for the liquid Cerenkov angle to $\sim \pm$ 0.5%. Such performance allows π, K, ρ separation over most of the momentum range of Z^0 decays. The SLD CRID experiment has demonstrated that it can resolve neighboring photoelectron hits (with the second pulse only 10% in amplitude of the first) within 3–4 mm.

Status of the Experiments

Delphi

▷ The LEP machine is planned to turn on in July 1989.

▷ The RICH subsystem is now being installed in DELPHI.

▷ At least part of the RICH will be operational at the turn-on of DELPHI.

SLD

o The SLC is running now, and we are hoping for the first Z^0's now.*

o The SLD experiment is coming together well. The magnet has been ready for over a year, and the muon system and tail-catcher calorimeter are ready. The Liquid Argon Calorimeter is being installed now and should be ready for cool-down by this Fall. The Central Tracker is finished stringing and should be ready for installation in the Fall. The Cerenkov counter vessel will be installed in SLD this Summer, and part [30–50%] of the components will be inserted by this Fall. The SLD will then prepare for a cosmic ray shakedown test in January-April 1990.

---

* **The first Z° from SLC was observed by Mark II on April 14,** 1989—seven **days after this talk.**

- The remainder of the CRID components will be installed in SLD following the cosmic ray test run, in Spring 1990.
- SLD should move into the beamline in SLC during the summer of 1990. It is expected that the removal, of Mark II, the installation of the new SLC Final Focus, and the roll-in of the SLD experiment will take about three months.

Conclusion

The two 4π Cerenkov ring imaging detectors are coming together quite rapidly and successfully. They promise to do their jobs well in a physics environment where they clearly have a lot to offer.

References

1. Delphi Proposal, LEPC 83-3 and LEPC 84-16.
2. SLD Design Report, SLAC-Report-273 (1984).
3. W. Atwood, private communication. Also discussed in D. Leith "Advances in Experimental Methods for Colliding Beam Physics," Nucl. Inst. Meth. A265, 120 (1988).
4. V. Ashford et al., published in Proc. XXIII Int. Conf. on High Energy Physics, Berkeley, CA, July 16-23, 1986 p. 1470.
5. T. Ypsilantis and J. Sequinot, this Symposium.
6. R. T. Rewick et al., Anal. Chem. 60, 2095 (1988), SLAC-PUB-4115.
7. T. Ypsilantis, invited talk at the Int. Conf. on Experiments at LEP, Physica Scripta, Vol. 1, 370 (1981).
8. T. Ekelof, Proceedings of the 1984 SLAC Summer Institute, SLAC–Report–281, 244 (1985).
9. Baillon et al., Nucl. Instr. Meth. A277, 338 (1989), and Nucl. Instr. Meth. A276, 492 (1989).
10. R. Arnold et al., Nucl. Instr. Meth. A270, 255 (1988).
11. D. Aston et al., presented at the Int. --Wire Chamber Conference, Vienna; February 13-17, 1989; SLAC-PUB-4875.
12. P. Coyle et al., internal CRID No. 58, "Photon Feedback Measurements in the Barrel CRID Detectors," (1989).
13. J. Va'vra, IEEE Trans. Nucl. Sci. NS-34, 1987; SLAC-PUB-4116 (1986).

Figure Captions

Fig. 1. A schematic quadrant view of the SLD detector at SLAC.

Fig. 2. Demonstration of the principle of the DELPHI and SLD Cerenkov Ring Imaging Detectors. (a) shows the arrangement of the two radiators and the photon detector; (b) shows the details of the long drift photoelectron detector.

Fig. 3. The particle identification performance expected for the Cerenkov Ring imaging Detector in DELPHI and SLD.

Fig. 4. The evolution of the charm signal in $K\pi\pi$ from Z^0 decays, from a Monte Carlo study by W. Atwood. The precision CCD vertex and the CRID system are used first separately and then together to isolate, with fair efficiency, a very clean D peak.

Fig. 5. Experimental data from test beam studies on the π K separation achieved by the SLD CRID prototype at 11 GeV/c.

Fig. 6. Schematic diagram of the mechanical layout of the SLD CRID.

Fig. 7. Estimated particle separation as a function of momentum with (a) the gas radiator and with (b) the liquid radiator. Indicated are la separation bands expected at the SLD, based on the prototype results.

Fig. 8. (a) Surface flatness measurements of the mirror blanks from Lancaster Co. They typically have 20-30 Å feature size: (b) The measured reflectance of the first 100 mirror blanks coated by Acton Co. for the SLD-CRID.

Fig. 9. Schematic diagram of the parallax error introduced by the Cerenkov photon attenuation length in the drift gas.

Fig. 10. Diagrammatic representation of photon feedback. First the Cerenkov photon is absorbed by a TMAE molecule in the drift gas and frees a photoelectron. The electron drifts under the action of a guide field to the high electric field region around an anode wire and experience a Townsend avalanche. The gas around the avalanche region is in an excited state and part of the time de-excites by emission of an optical photon. Such photons are quickly absorbed in the high quantum efficiency photocathode gas, thus giving use to a positive feedback mechanism. For successful operation of a Cerenkov Ring Imaging Detector this phenomena must be tamed.

Fig. 11. A Schematic of the DELPHI electron detector showing the blinds between anode wires which control the photon feedback.

Fig. 12. A schematic of the SLD electron detector showing the teched arrays and U-shaped cathode which control the photon feedback.

Fig. 13. The measured photon feedback in the SLD electron detector as a function of chamber voltage.

Fig. 14. The measured charge division resolution in the SLD electron detector.

Fig. 15. The position resolution as a function of distance along the anode wire for the SLD detector.

Fig. 16. Gas chromatograph traces for (a) commercial TMAE, and (b) TMAE washed and passed through a sieve.

Fig. 17. A photograph of the core of an SLD drift box during assembly.

Fig. 18. Trajectories for electrons and positrons near the electron detector in the SLD for open and closed gate voltage settings.

Fig. 19. Photograph of the deposit on an anode wire after aging and opening to the atmosphere.

Fig. 20. Data on the aging cycle of an SLD electron detector with TMAE being repeatedly aged by exposure to radiation and "cleaned" by locally heating the anode.

Fig. 21. Comparison of the measured and calculated Cerenkov angular resolution, for both liquid and gas radiators in the DELPHI RICH prototype.

Fig. 22. Single event display from the SLD CRID prototype; (a) and (b) are 11 GeV/c π^+ and K^+, respectively, while (c) and (d) are 4 GeV/c π^- and e^-, respectively.

Table I

Radiator Choices for Four **Čerenkov** Ring Imaging Detectors.

Radiator	n	γ_{th}	**Pion** Threshold **(GeV/c)**	Number of photoelectrons from L_{cms} of Radiator	Experiment Goals
Helium	1.000038	116	16	**(TEA)** 6 from 1500 **cms**	E-605 π, K, p (50-200) **GeV/c**
Nitrogen	1.00032	40	5.5	(TMAE) 28 from 500 **cms**	RAL-Omega A, K, p (20-150) **GeV/c**
C_5F_{12}	1.0017	17	2.4	(TMAE) 12 **from** 45 **cms**	SLD/DELPHI Z^0 decays e, π, K, p **(1/2-40) GeV/c**
C_6F_{14}	1.2176	1.5	0.2	(TMAE) 24 from 1 cm	

Table II

Comparison of TEA **and** TMAE Photocathodes

	TEA	TMAE
Absorption Length for **Čerenkov** Light	1 mm	(15-40) mm depending on temp.
High Edge of Wavelength Window	around 1500 Å	around 1950 Å
Requirement in O_2, H_2O	$\leq$ 200 ppb	$\leq$ 20 ppm
Window Material	CaF	Quartz

Table III

Choices of “Principle” for the Ring Imaging Detector

COMPONENT	**SLD**	**DELPHI**
Radiator	1 cm C_6F_{14} 45 cm C_5F_{12}	
Photocathode	TMAE at 28°C	
Optics	Spherical, Ground and Polished Mirrors	Parabolic, Slumped Glass
	Proximity Focusing for Liquid	Same
Electron Detector	MWPC with Resistive Anode	MWPC
	Charge Division for Third Coordinate	Cathode Strips
	Forward and Side Blinding ($\theta \sim 6°$)	Side Blinds ($\theta \sim 14°$)

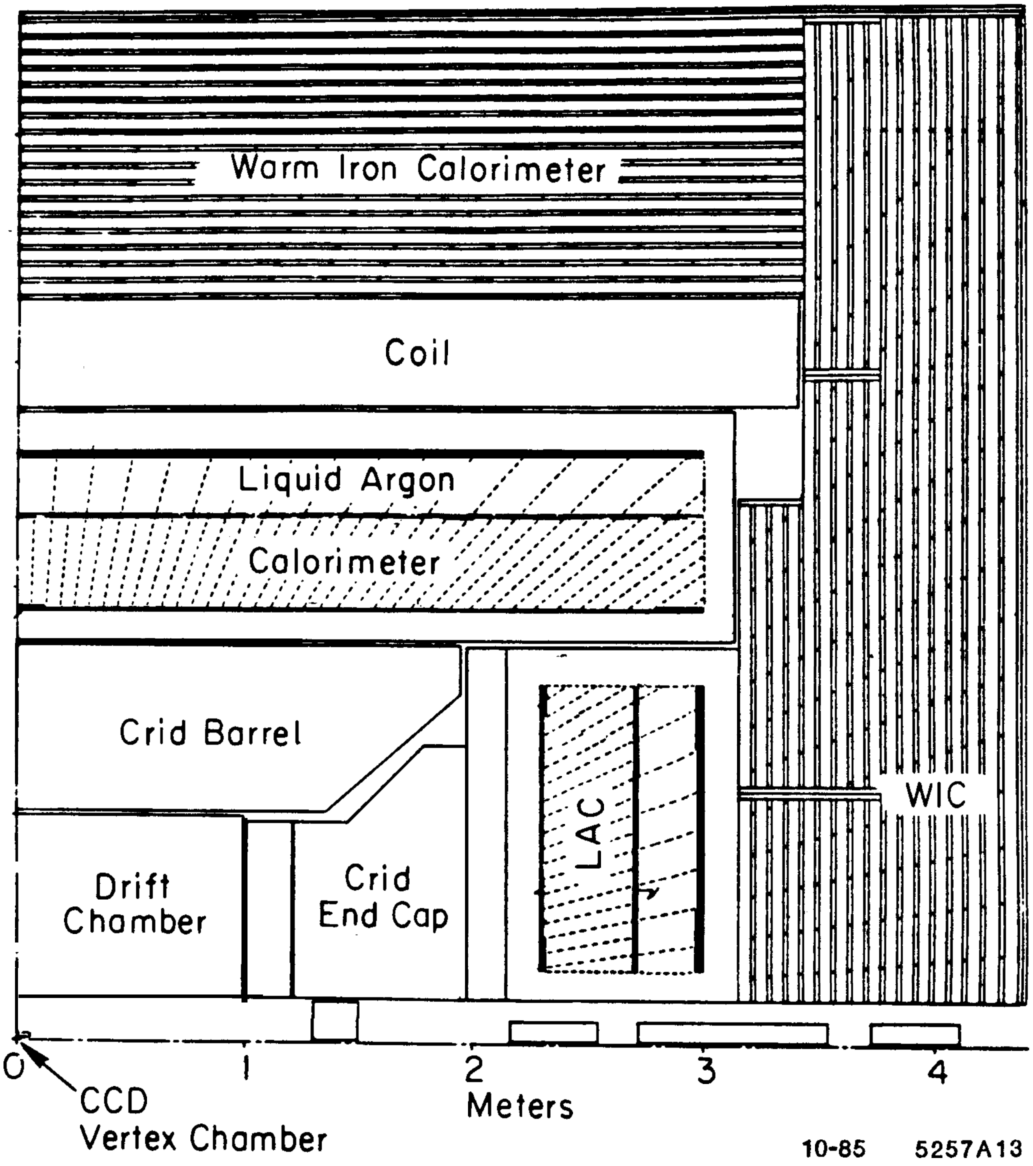
Warm Iron Calorimeter
Coil
Liquid Argon
Calorimeter
Crid Barrel
Drift
Chamber
Crid
End Cap
LAC
WIC
0
1
2
3
4
Meters
CCD
Vertex Chamber
10-85
5257A13

Fig. 1

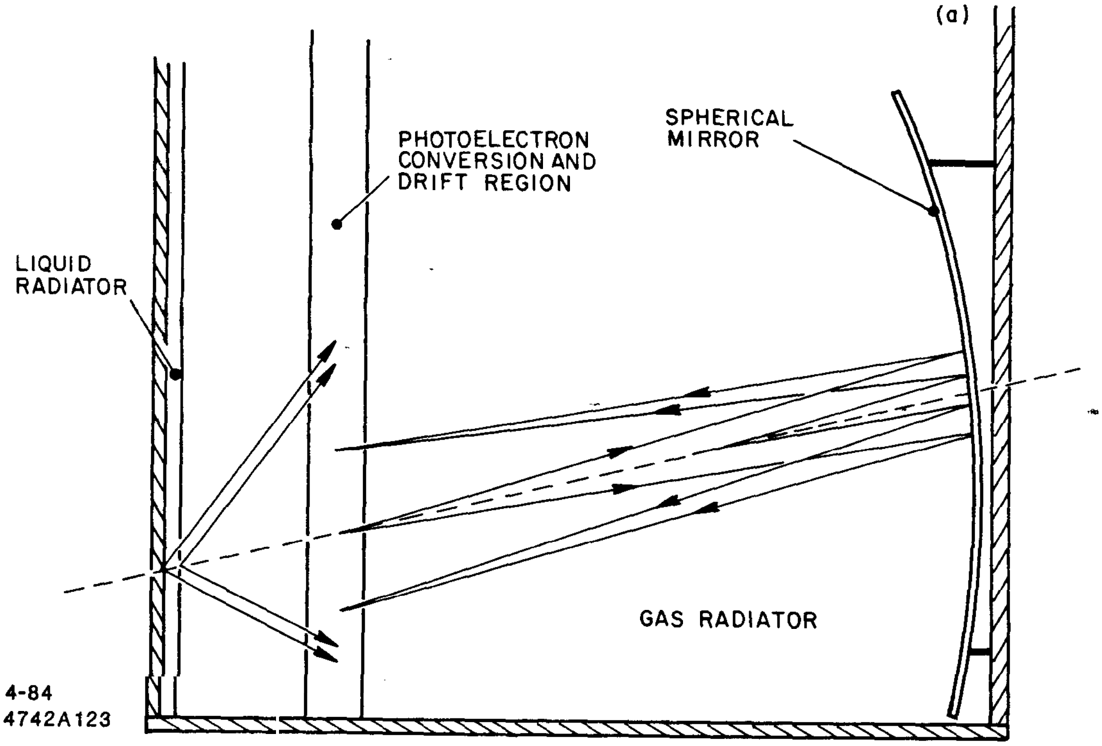
(a)
SPHERICAL MIRROR
PHOTOELECTRON CONVERSION AND DRIFT REGION
LIQUID RADIATOR
GAS RADIATOR
4-84
4742A123

Fig. 2a

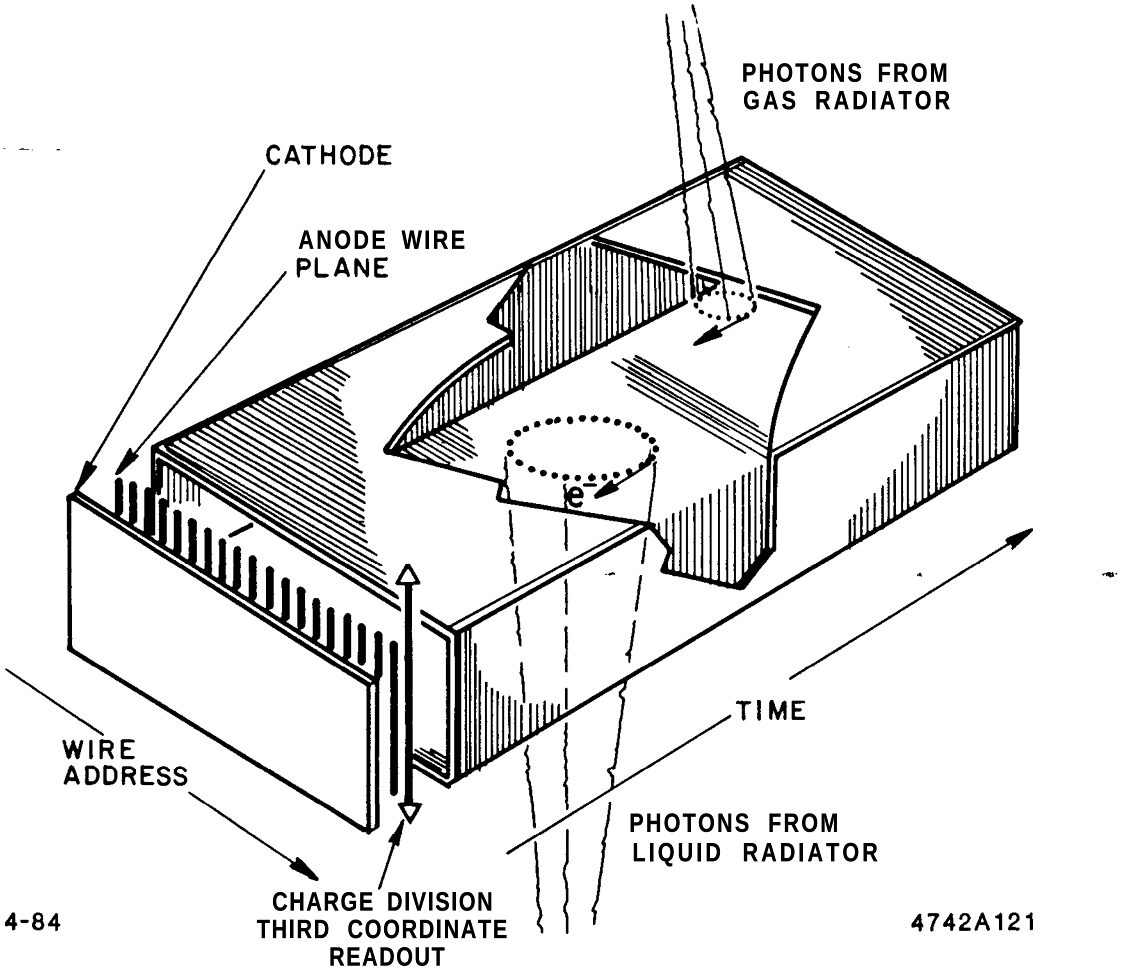

PHOTONS FROM
GAS RADIATOR
CATHODE
ANODE WIRE
PLANE
e⁻
TIME
WIRE
ADDRESS
PHOTONS FROM
LIQUID RADIATOR
CHARGE DIVISION
THIRD COORDINATE
READOUT
4-84
4742A121

Fig. 2b

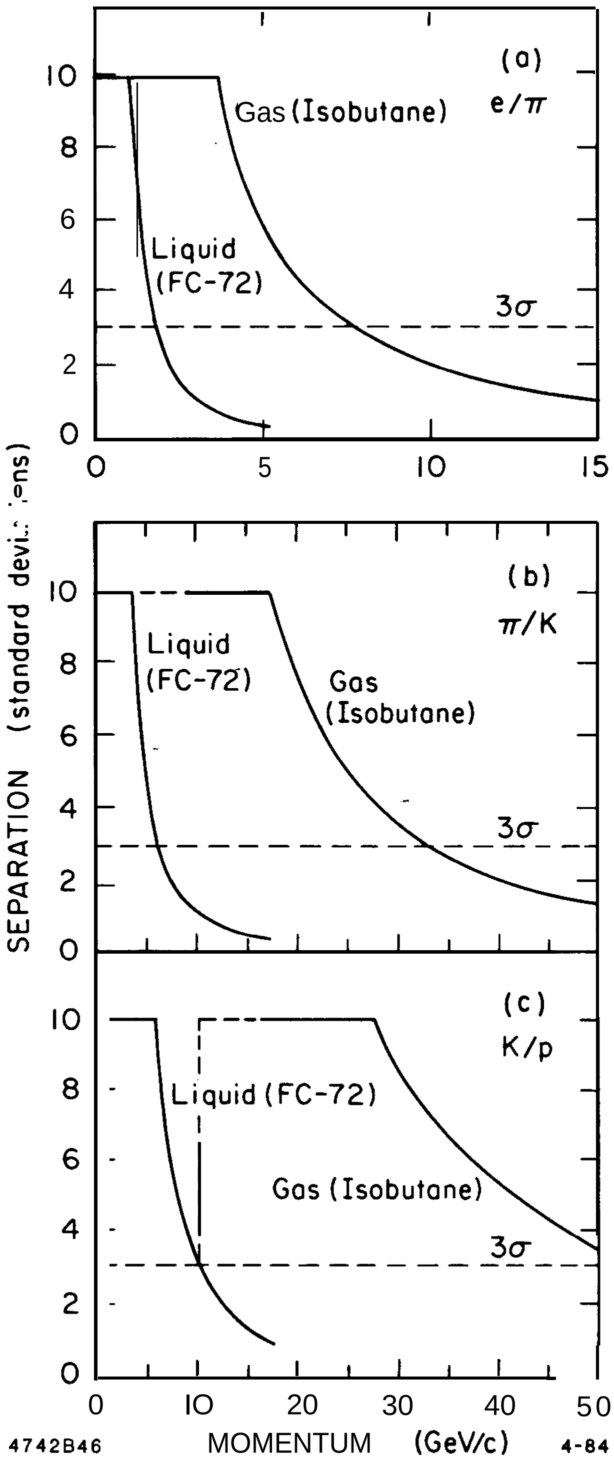
(a)
e/π
Gas (Isobutane)
Liquid (FC-72)
3σ
(b)
π/K
Liquid (FC-72)
Gas (Isobutane)
3σ
(c)
K/p
Liquid (FC-72)
Gas (Isobutane)
3σ
SEPARATION (standard deviations)
0
2
4
6
8
10
0
5
10
15
0
10
20
30
40
50
MOMENTUM (GeV/c)
4742B46
4-84

Fig. 3

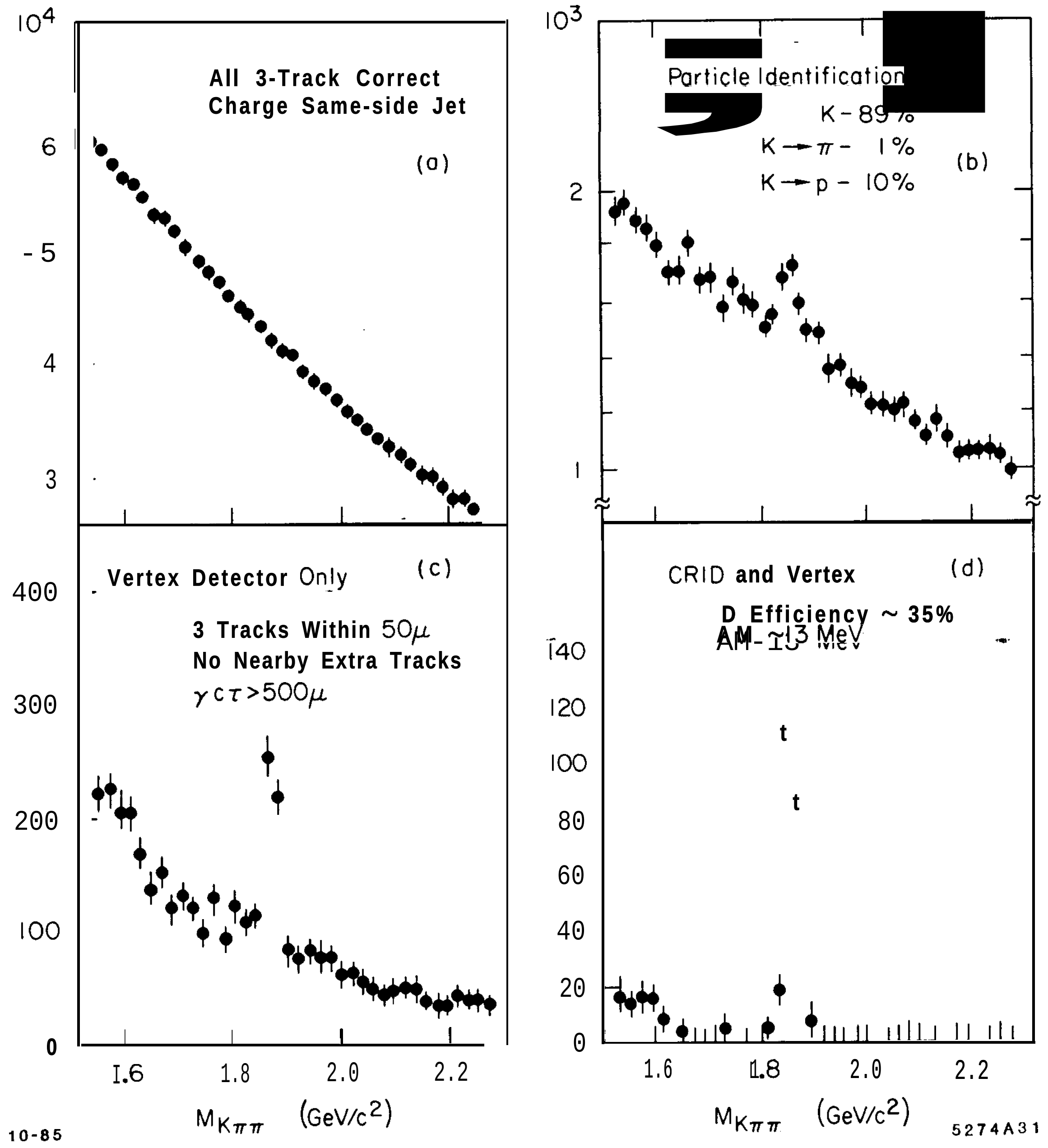

10^4
6
5
4
3
All 3-Track Correct
Charge Same-side Jet
(a)
10^3
2
1
Particle Identification
K - 89%
$K \rightarrow \pi$ - 1%
$K \rightarrow p$ - 10%
(b)
400
300
200
100
0
Vertex Detector Only
(c)
3 Tracks Within 50μ
No Nearby Extra Tracks
$\gamma c\tau > 500\mu$
140
120
100
80
60
40
20
0
CRID and Vertex
(d)
D Efficiency ~ 35%
ΔM ~13 MeV
1.6
1.8
2.0
2.2
$M_{K\pi\pi}$ (GeV/c^2)
10-85
5274A31

Fig. 4

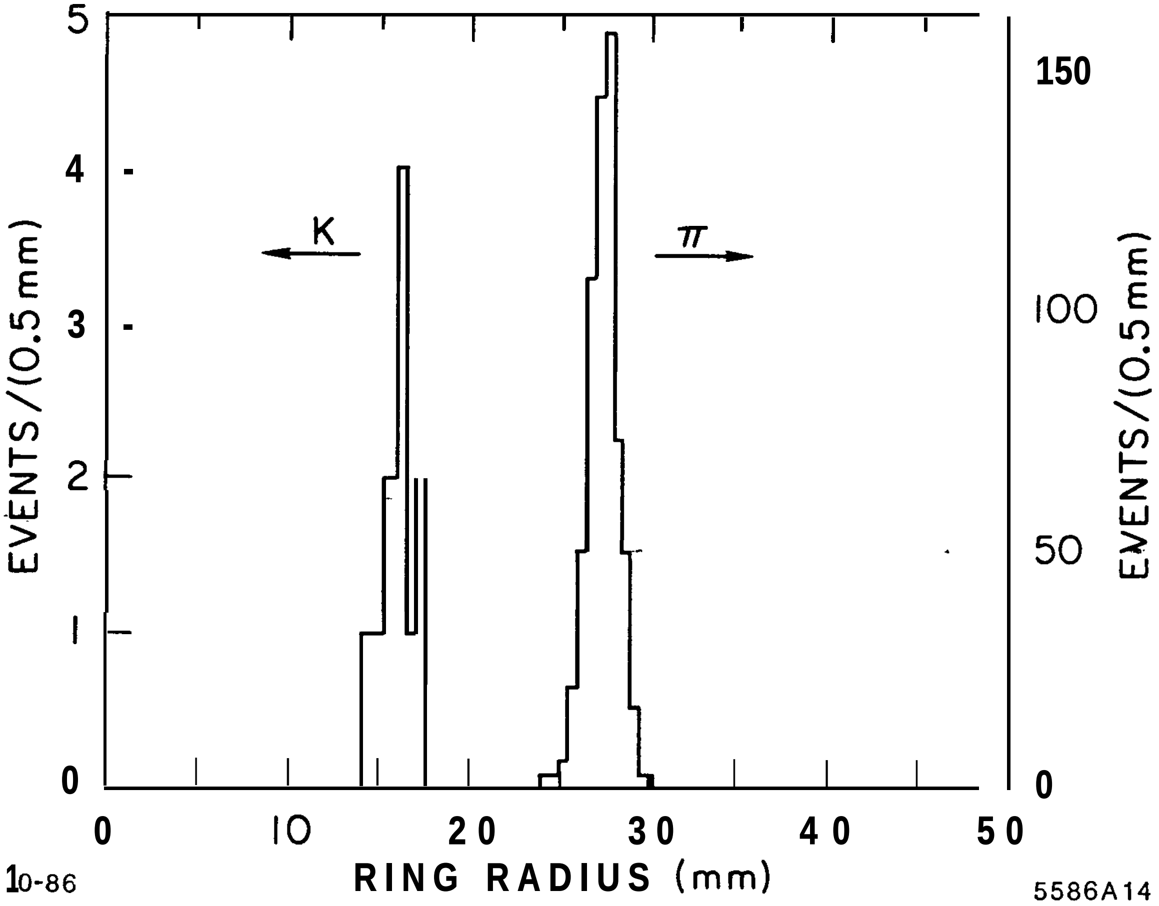
5
4
3
2
1
0
EVENTS/(0.5 mm)
K
π
150
100
50
0
EVENTS/(0.5 mm)
0
10
20
30
40
50
RING RADIUS (mm)
10-86
5586A14

Fig. 5

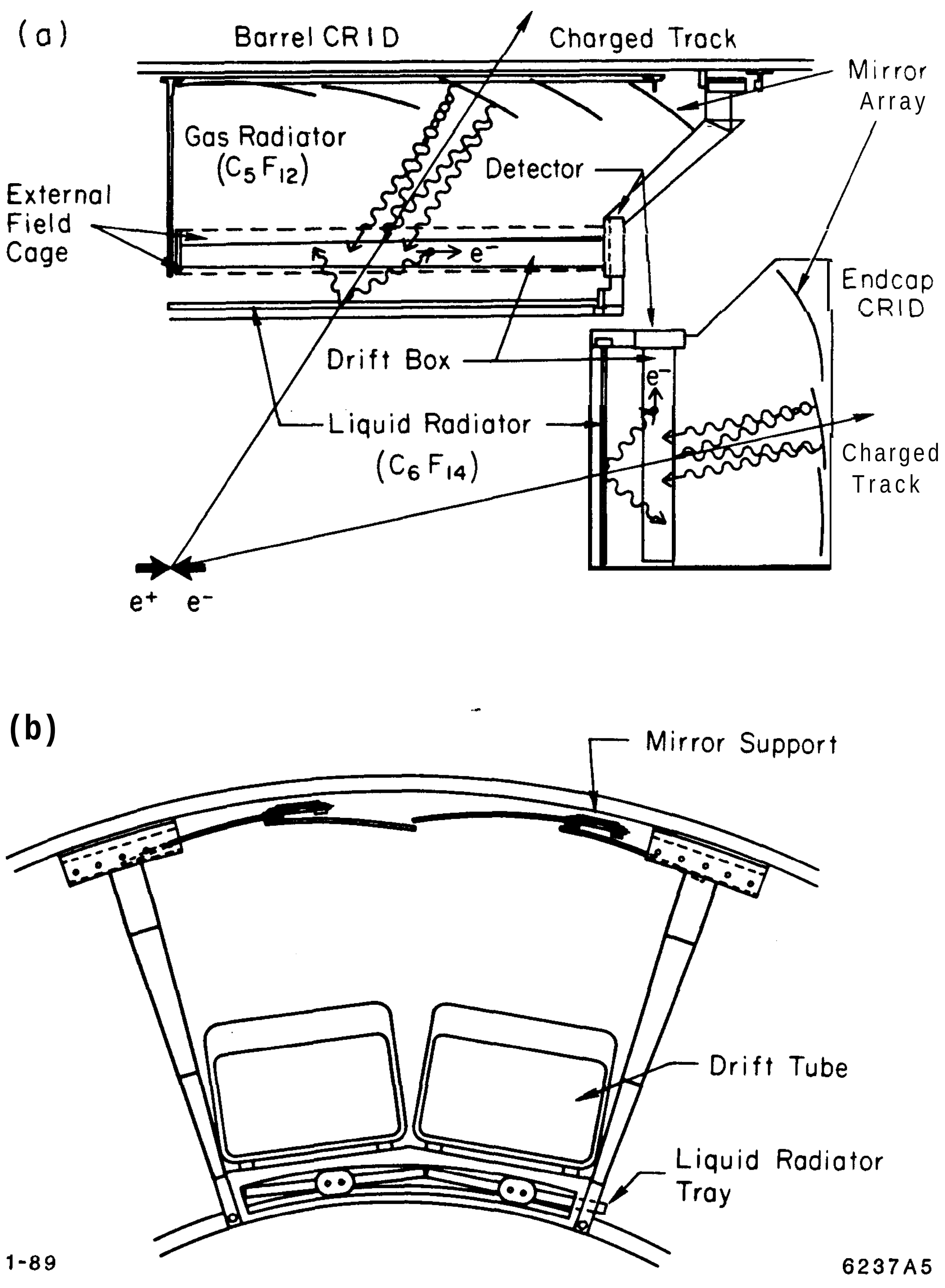
(a)
Barrel CRID
Charged Track
Mirror Array
Gas Radiator (C_5F_{12})
Detector
External Field Cage
e⁻
Endcap CRID
Drift Box
e⁻
Liquid Radiator (C_6F_{14})
Charged Track
e⁺ e⁻
(b)
Mirror Support
Drift Tube
Liquid Radiator Tray
1-89
6237A5

Fig. 6

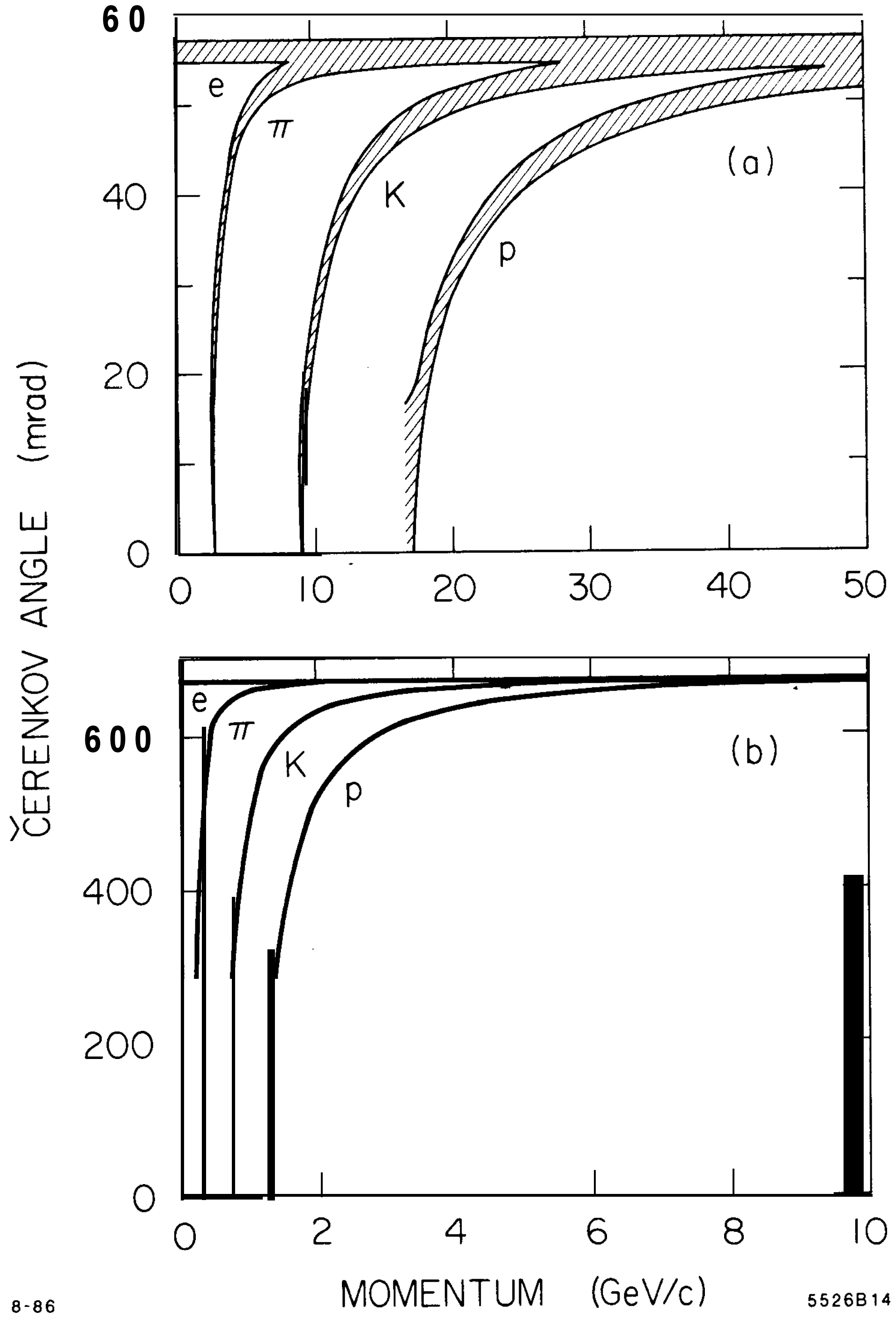

60
40
20
0
e
π
K
p
(a)
0
10
20
30
40
50
ČERENKOV ANGLE (mrad)
600
400
200
0
e
π
K
p
(b)
0
2
4
6
8
10
MOMENTUM (GeV/c)
8-86
5526B14

Fig. 7

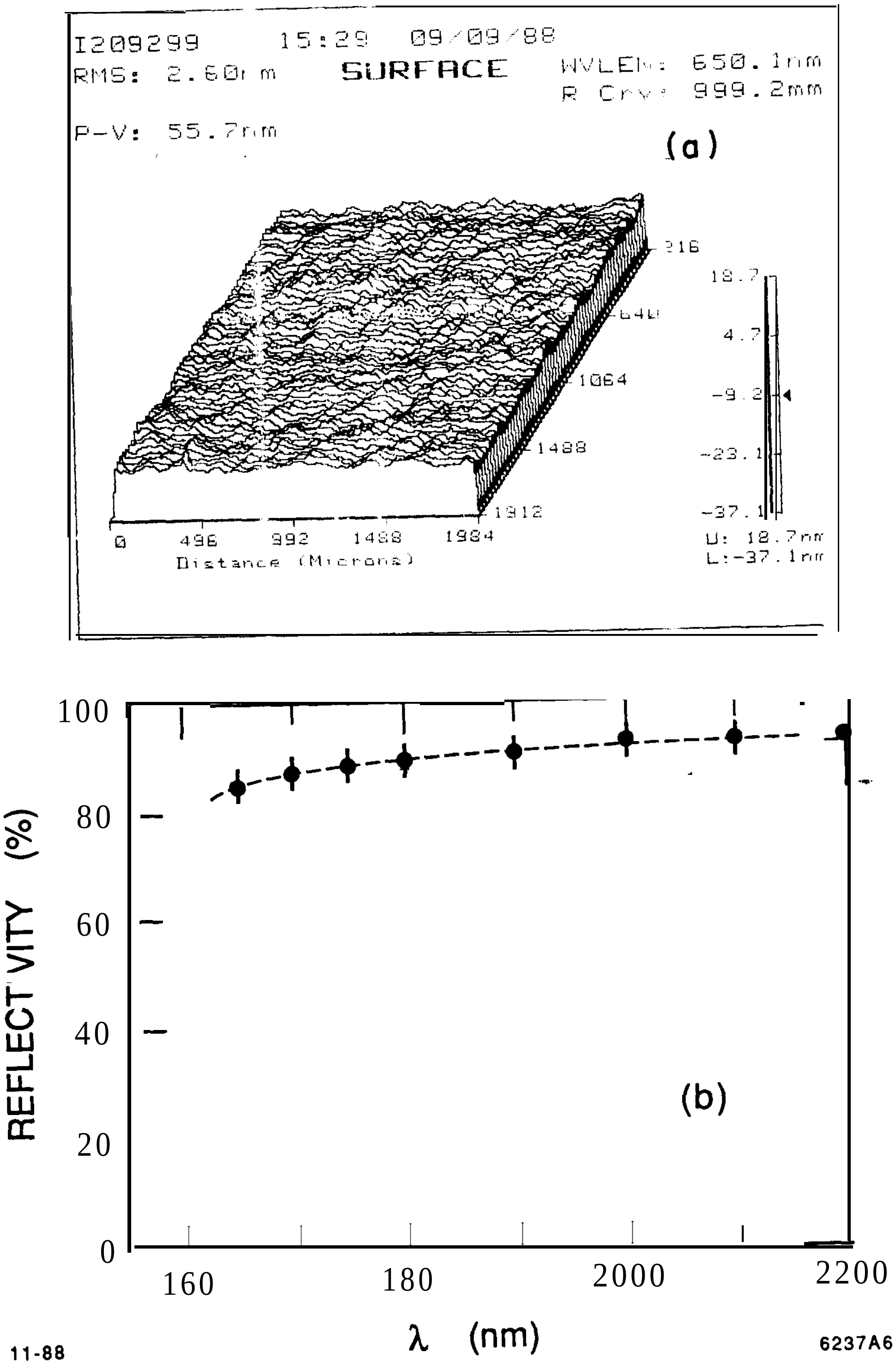
I209299 15:29 09/09/88
RMS: 2.60nm
SURFACE
WVLEN: 650.1nm
R Crv: 999.2mm
P-V: 55.7nm
(a)
216
640
1064
1488
1912
18.7
4.7
-9.2
-23.1
-37.1
0
496
992
1488
1984
Distance (Microns)
U: 18.7nm
L: -37.1nm
100
80
60
40
20
0
REFLECTIVITY (%)
(b)
160
180
2000
2200
λ (nm)
11-88
6237A6

Fig. 8

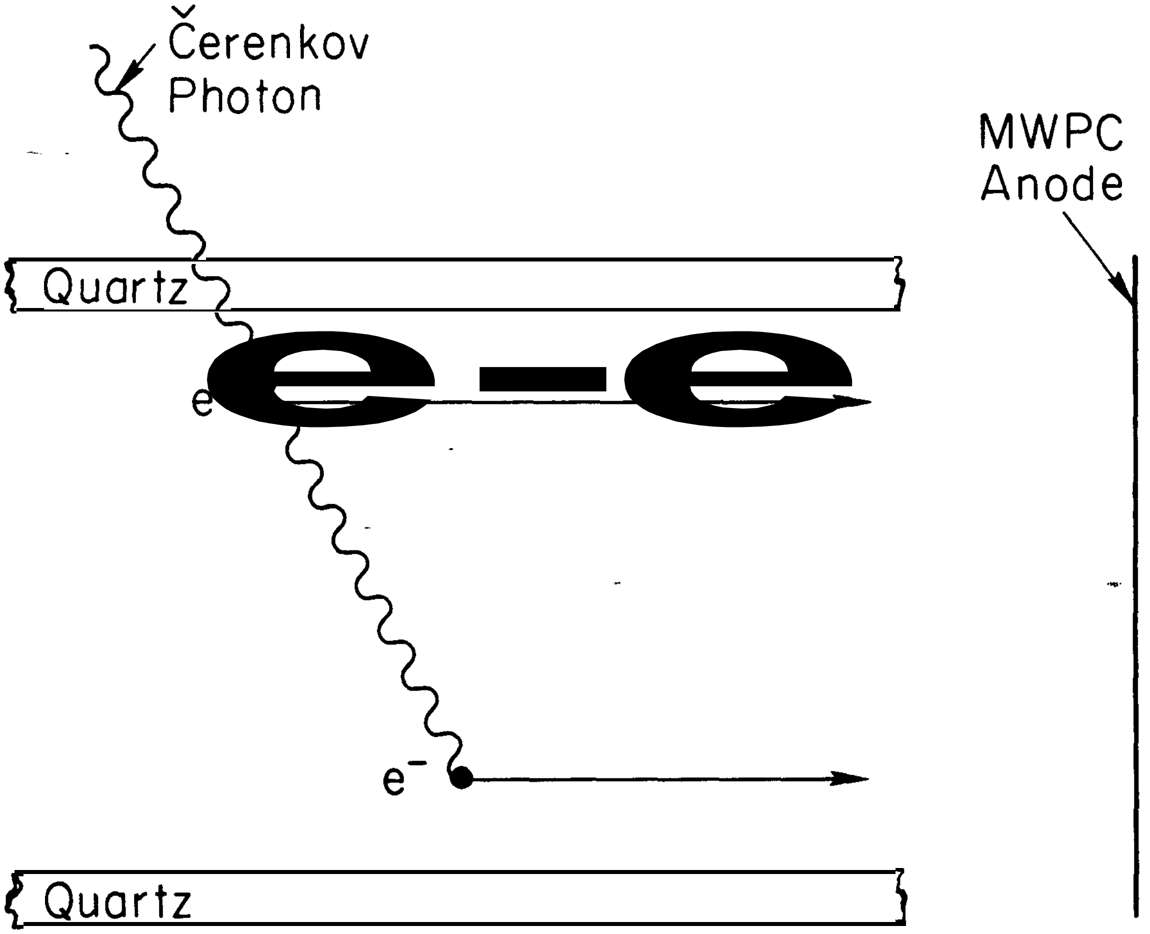

6-87

5804A4

Fig. 9

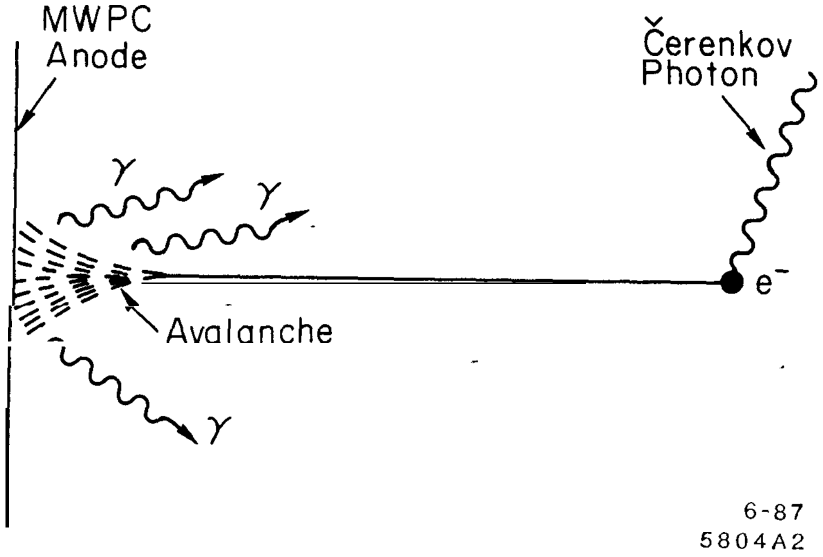

Fig. 10

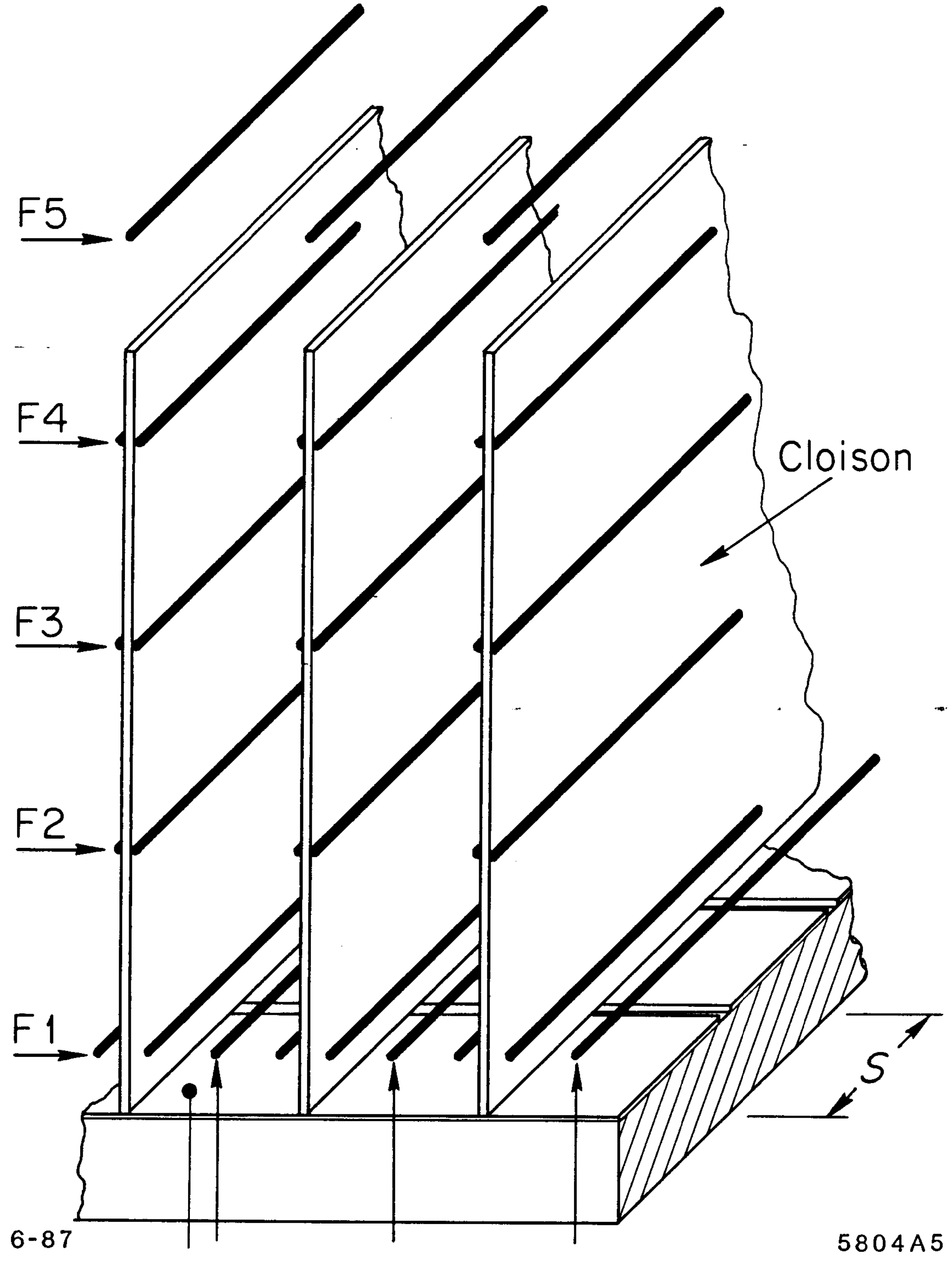

Fig. 1

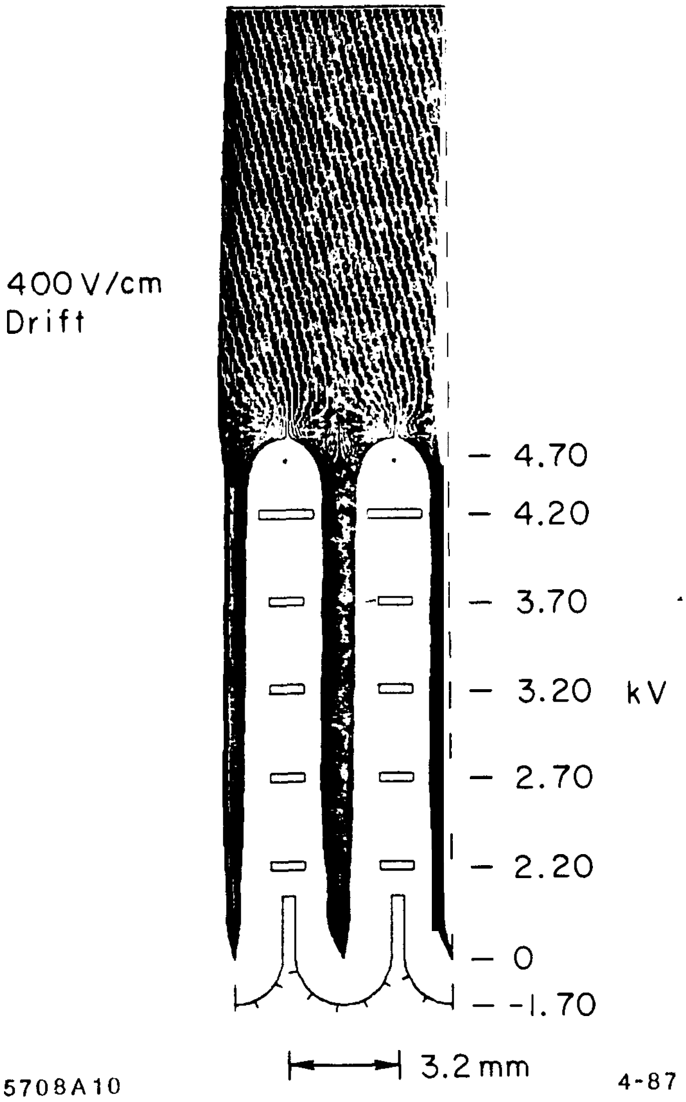

Fig. 12

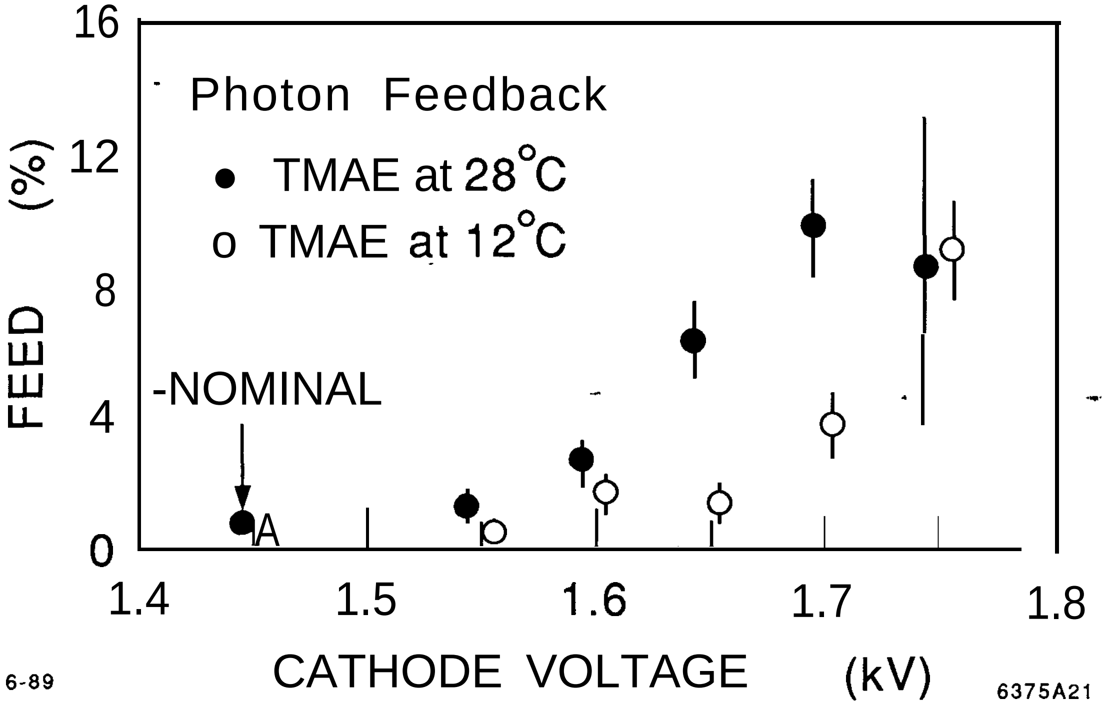

Photon Feedback
● TMAE at 28°C
o TMAE at 12°C
-NOMINAL
A
FEED (%)
0
4
8
12
16
1.4
1.5
1.6
1.7
1.8
CATHODE VOLTAGE (kV)
6-89
6375A21

Fig. 13

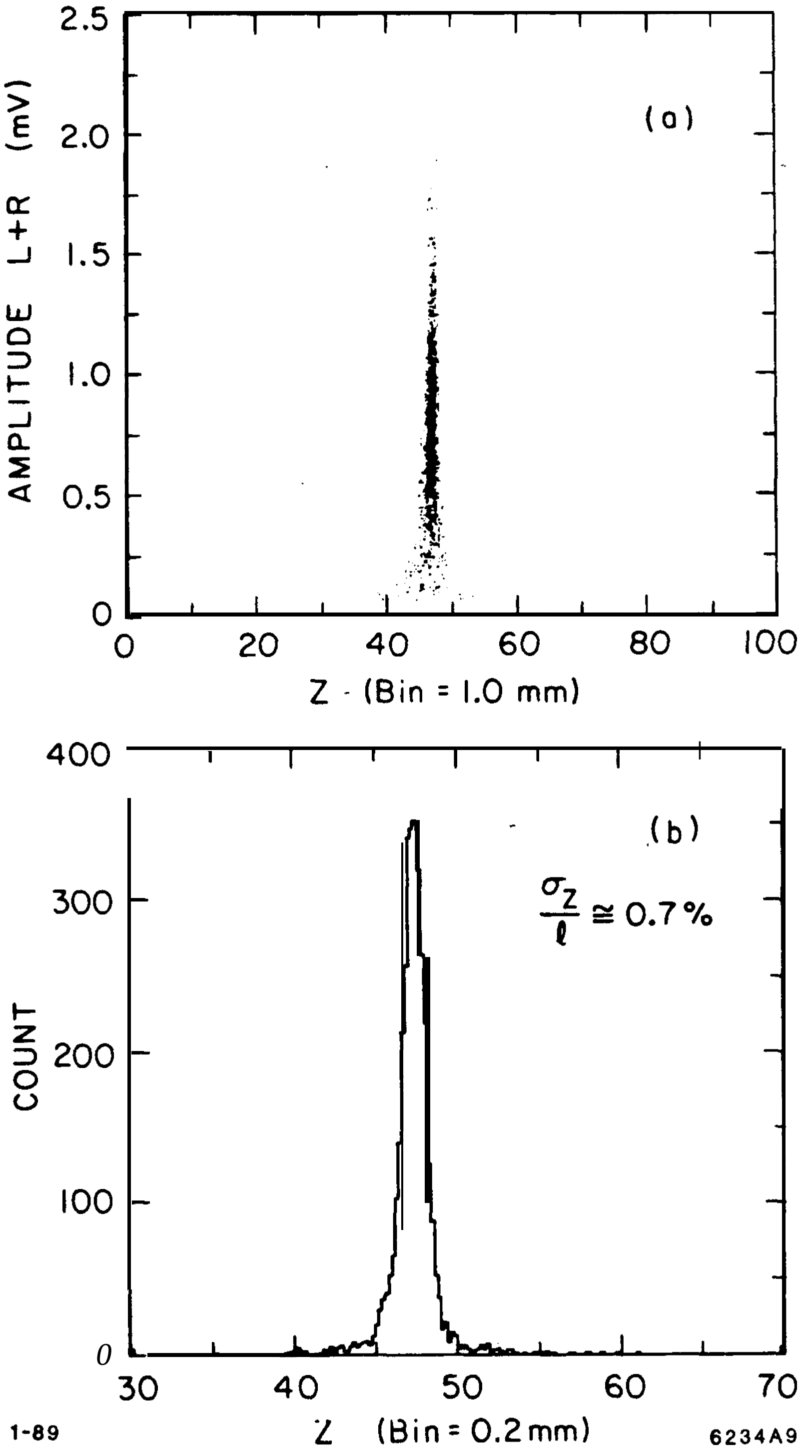
2.5
2.0
1.5
1.0
0.5
0
AMPLITUDE L+R (mV)
(a)
0
20
40
60
80
100
Z - (Bin = 1.0 mm)
400
300
200
100
0
COUNT
(b)
$\frac{\sigma_Z}{\ell} \cong 0.7\%$
30
40
50
60
70
Z (Bin = 0.2 mm)
1-89
6234A9

Fig. 14

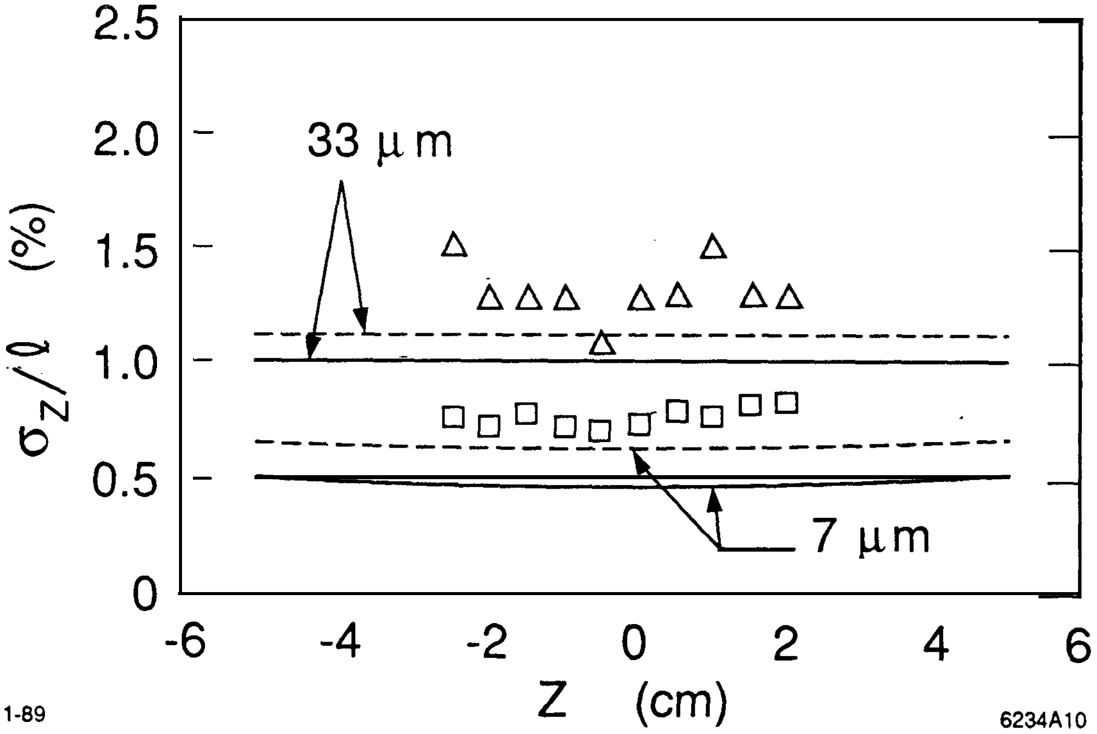

Fig. 15

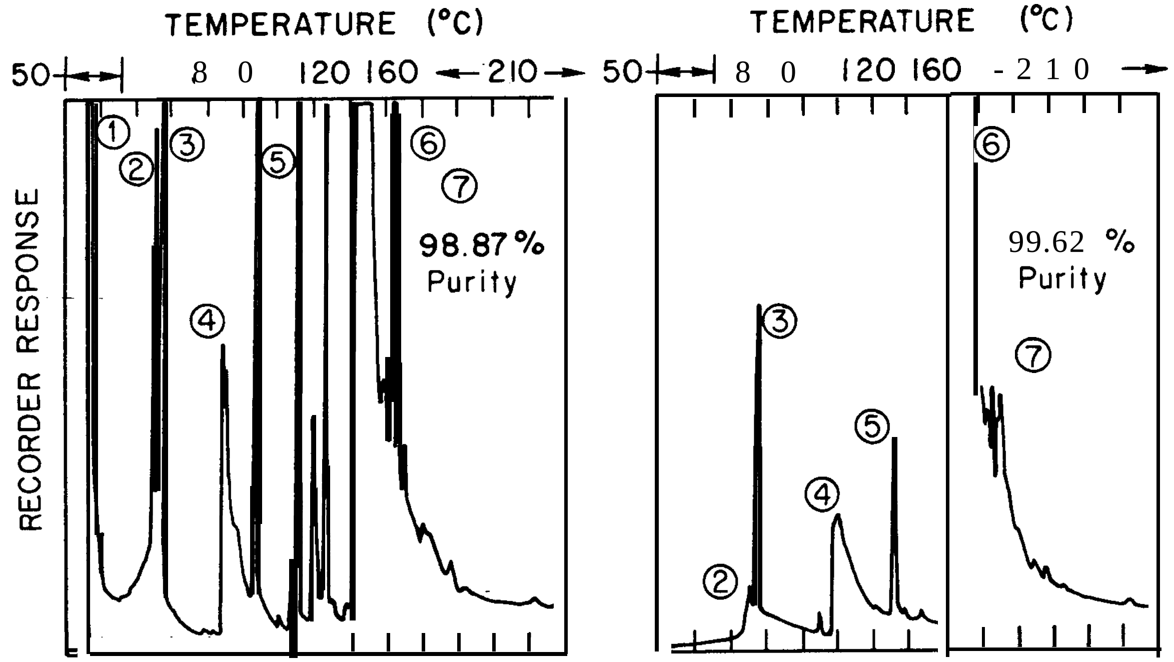

(a) As Received from RSA Corp

(b) Washed with Water and Passed through a Molecular Sieve

Symbol Identification

Symbol	**Name**	Formula	MW
DMA	Dimethylamine	$(CH_3)_2NH$	**45**
TMH	Tetramethylhydrszine	$(CH_3)_2 - N - N(CH_3)_2$	**88**
BMAM	Bis(dimethylamino)methane	$[(CH_3)_2N]_2 - CH_2$	102
DMF	Dimethylformamide	$H(C = O) - N(CH_3)_2$	73
TMU	Tetramethylurea	$[(CH_3)_2N]_2 - C = O$	116
TMAE	Tetrakis(dimethylamino)ethylene	$C_2[(CH_3)_2N]_4$	200
TMO	Tetramethyloxamide	$[(CH_3)_2N]_2 - (C = O)_2$	144

6-87

5804A28

Fig. 16

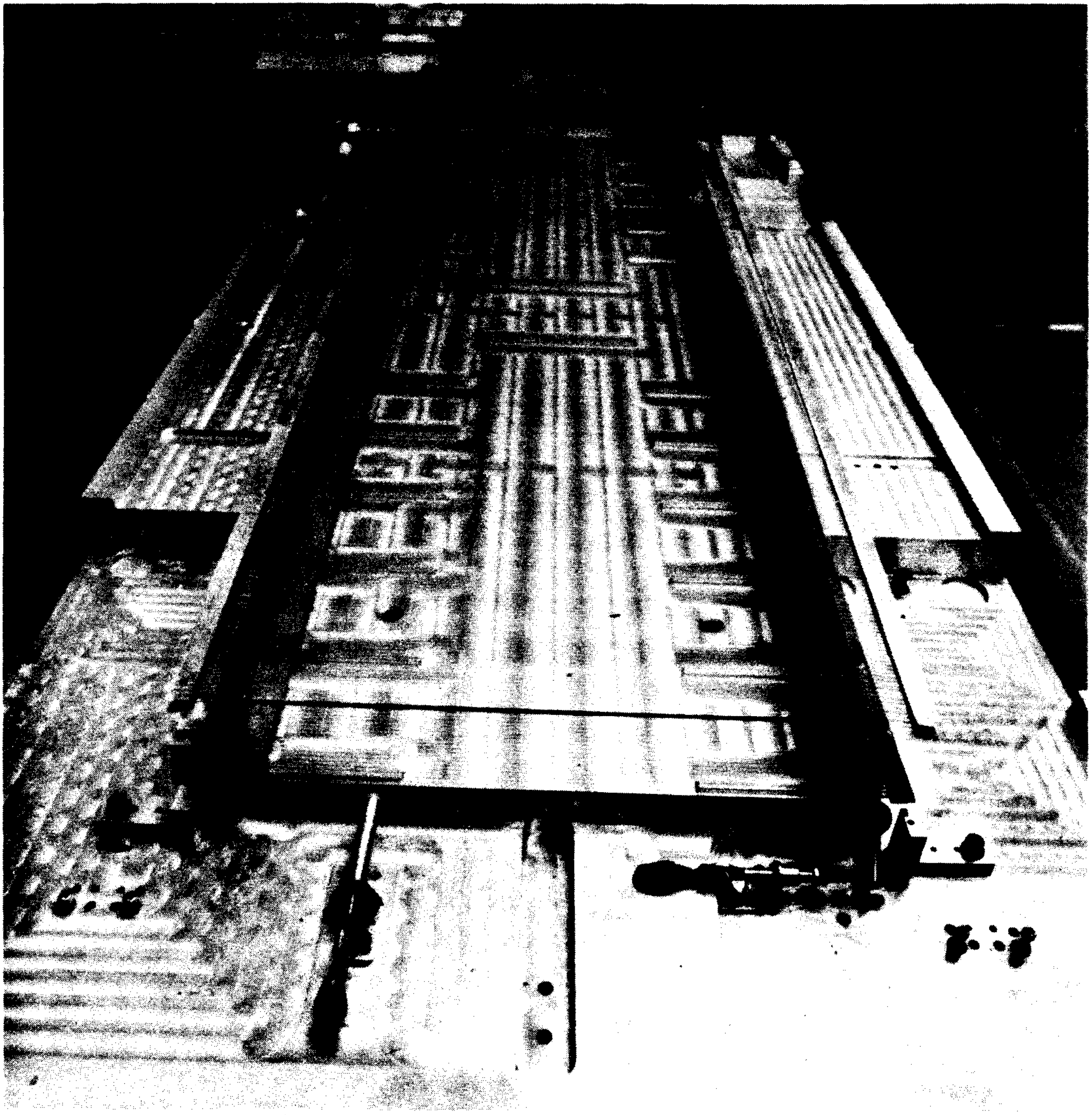

Fig. 17

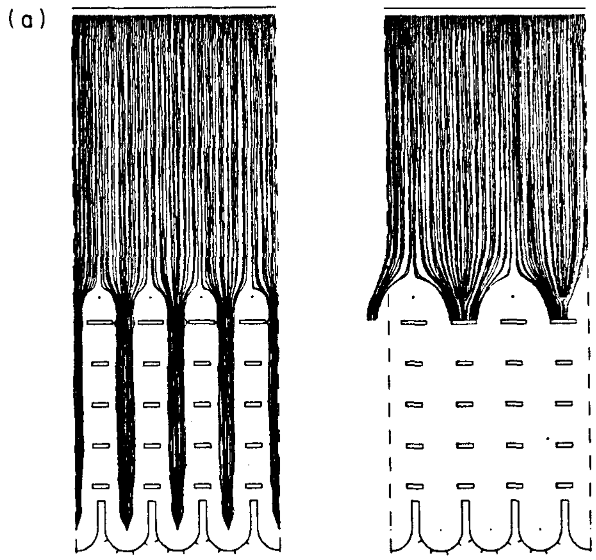

Nominal Electron Drift Trajectories

Electron Drift Trajectories with the Gating On (± 350 volts)

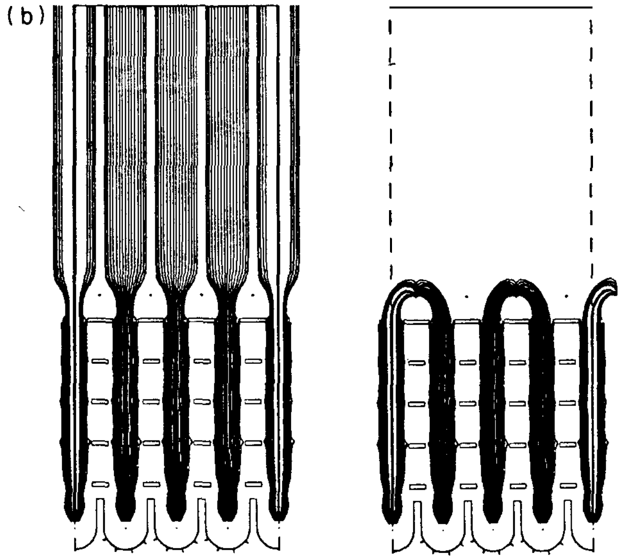

Nominal Positive Ion Trajectories

Positive Ion Trajectories with the Gating On (±350 volts)

10-88

6165B5

Fig. 18

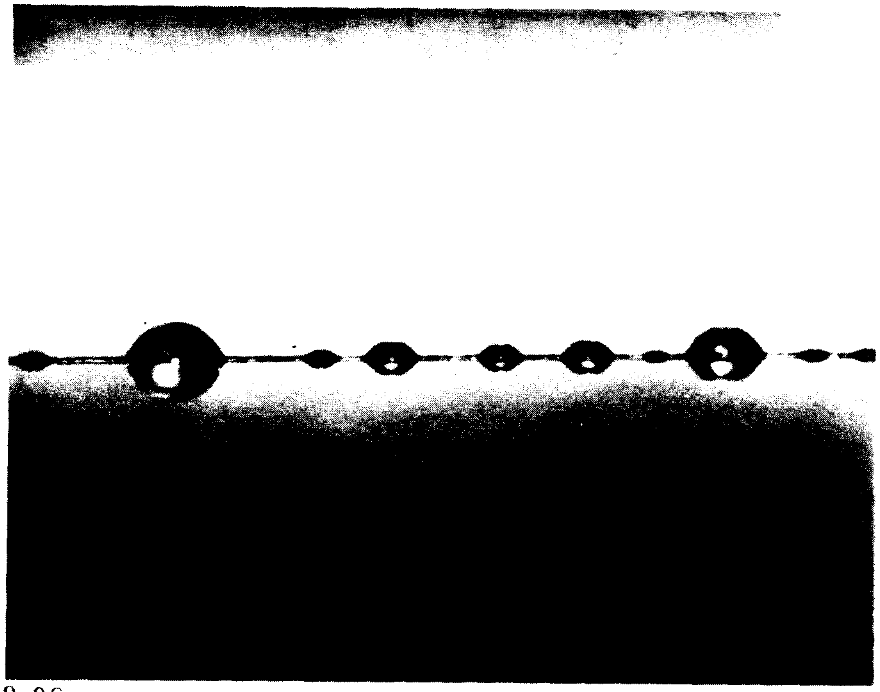

Fig. 19

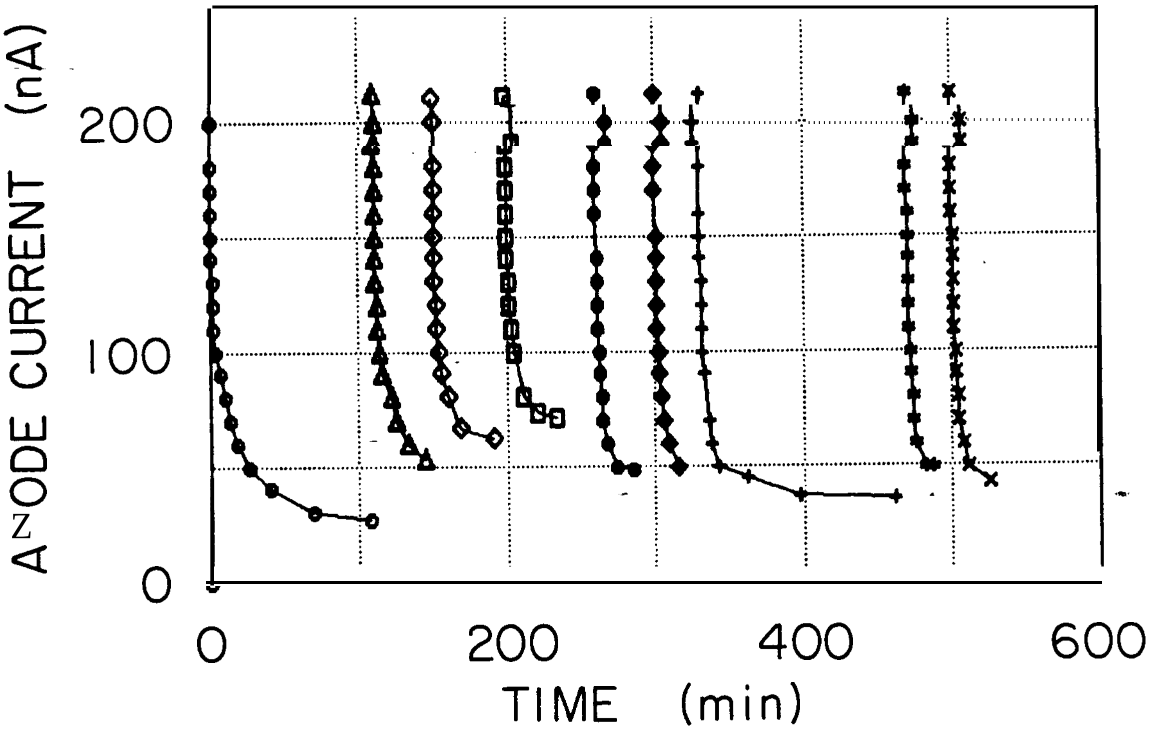

6-87
5804A6

Fig. 20

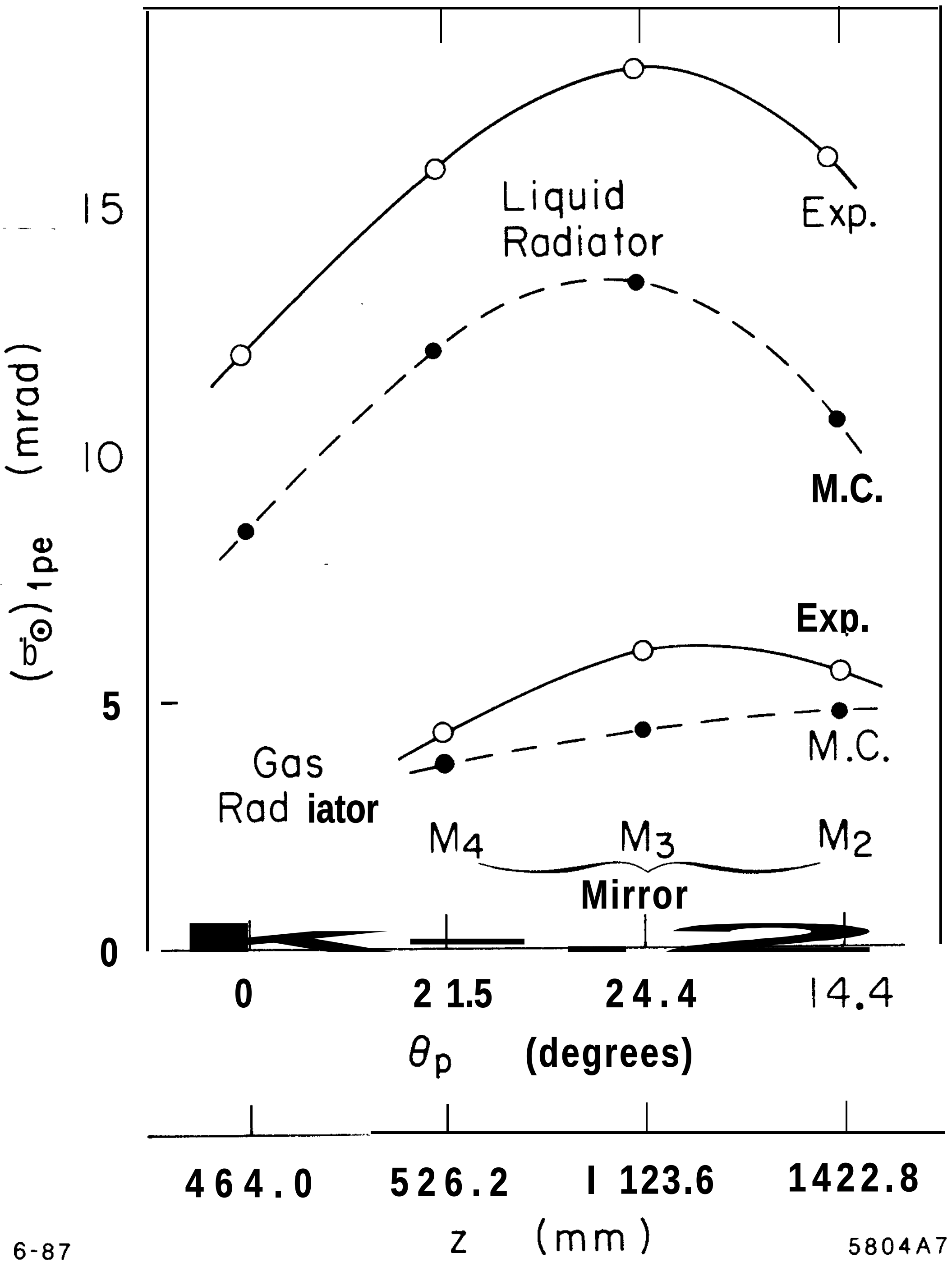
15
10
5
0
$(\bar{b}_{\odot})_{1pe}$ (mrad)
Liquid Radiator
Exp.
M.C.
Exp.
M.C.
Gas Radiator
M4
M3
M2
Mirror
0
21.5
24.4
14.4
θ_p (degrees)
464.0
526.2
1123.6
1422.8
z (mm)
6-87
5804A7

Fig. 21

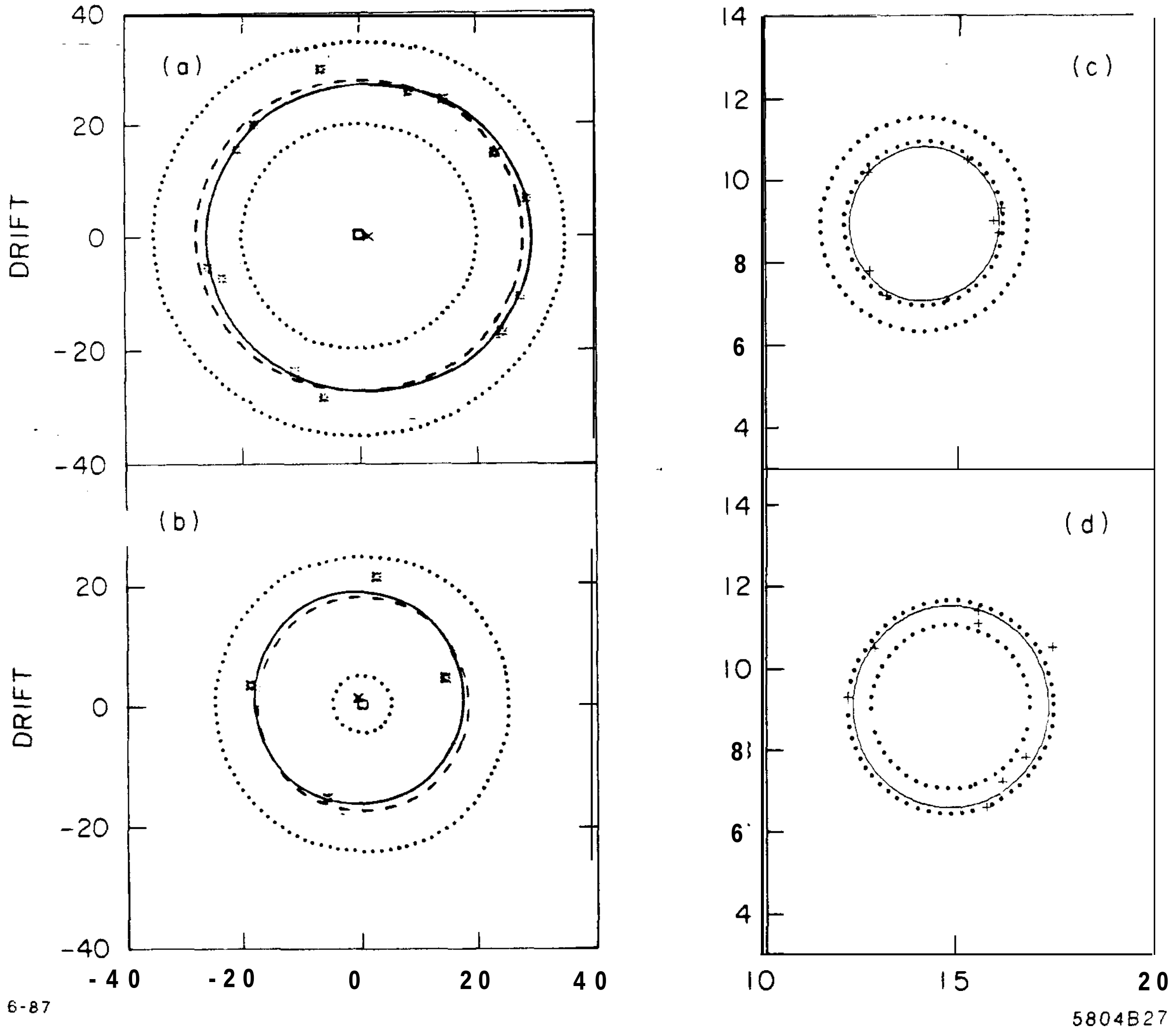
(a)
(b)
(c)
(d)
DRIFT
DRIFT
40
20
0
-20
-40
20
0
-20
-40
14
12
10
8
6
4
14
12
10
8
6
4
-40
-20
0
20
40
10
15
20
6-87
5804B27

Fig. 22